Construction and Building Materials 226 (2019) 888–898

Contents lists available at ScienceDirect

Construction and Building Materials

journal homepage: www.elsevier.com/locate/conbuildmat

Metallurgical characterisation of a historical metal tie-rod from Milan Cathedral

Mariagrazia Bellanova [a,*], Andrea Baggioli [b], Barbara Rivolta [c], Roberto Felicetti [a]

[a] Department of Civil and Environmental Engineering, Politecnico di Milano, Piazza Leonardo da Vinci, 32, 20133 Milano, Italy
[b] Polo Territoriale di Lecco, Politecnico di Milano, Via Gaetano Previati, 1/c, 23900 Lecco, Italy
[c] Dipartimento di Meccanica, Politecnico di Milano, Via La Masa 1, 20156 Milano, Italy

HIGHLIGHTS

- The metallurgical features of a hand-made tie were studied to infer the causes of failure.
- The material was found to be extremely heterogeneous in terms of matrix, inclusions and defects.
- Metallurgical evidence suggests that failure occurred along forged welds.
- More ductile behaviour is associated with a mainly ferritic matrix with iron-rich bulky-shape dendritic slag inclusions.
- Sudden variation of microstructure due to the forged weld can be seen across the visible crack.

ARTICLE INFO

Article history:
Received 12 February 2019
Received in revised form 3 July 2019
Accepted 22 July 2019

Keywords:
Tie-rod
Wrought-iron
Milan cathedral
Failure analysis
Metallurgical characterization
Archaeometallurgy

ABSTRACT

One tie-rod from Milan Cathedral (15th century) recently broke in a defective cross-section. In order to infer the causes of failure, a metallurgical characterisation was performed, the results of which are discussed here. First, a visual inspection of the specimen was performed. Next, the fracture surface was analysed using a Scanning Electron Microscope (SEM) combined with Energy Dispersive X-Ray Spectrometry (EDXS) to detect the failure modes involved. A cross-section close to the failure surface was investigated by means of Stereoscopy, Light Optical Microscopy (LOM), SEM and EDXS in order to identify the microstructural compounds and characterise the slag inclusions. Vickers and Rockwell hardness tests were also carried out to correlate microstructural observations with mechanical properties. A strong relationship between failure and defects due to forging was observed, which is a particularly noteworthy result with regard to the representativeness of laboratory tests and the viability of in-situ inspection.

1. Introduction

Historical wrought iron can be considered a completely different material from modern steel, despite both of them being iron-carbon alloys. Regarding iron-working technology, in the past no theoretical knowledge was available. Artisans learned to produce artefacts in workshops in accordance with the best practices available at the time. The quality of the products strongly depended on the master's ability. Therefore, workpieces from the same period may differ greatly from one another. Sometimes the main material properties may vary even within the same element.

Ore reduction and forging are probably the most crucial stages. Mechanical properties, homogeneity and surface features are highly dependent on the smelting temperature and reducing power of the furnace. In the history of metallurgy, two ore reduction methods can be distinguished: the direct and the indirect method, which have been extensively discussed by many authors [1,2]. The direct method is the most ancient technique. The reaction product is a spongy mass called bloom, which is a highly heterogeneous mixture of solid iron usually characterised by a large number of non-metallic Slag Inclusions (SIs), local porosities, and larger voids. The indirect method was introduced in the 14th century. The term refers to the reduction of ore into pig iron in the blast furnaces. This pig iron could be used for casting or reheated in finery forges. As many authors have pointed out, the metallurgical analysis of SIs can provide interesting information about the reduction method used [3,4]. With regard to the forging phase, macro discontinuities and rough surfaces resulted from

* Corresponding author.
E-mail addresses: mariagrazia.bellanova@polimi.it (M. Bellanova), andrea.baggioli@polimi.it (A. Baggioli), barbara.rivolta@polimi.it (B. Rivolta), roberto.felicetti@polimi.it (R. Felicetti).

https://doi.org/10.1016/j.conbuildmat.2019.07.272
0950-0618/

handwork. Typical macro-defects of tie-rods are forged welds. Wrought iron elements of considerable size (such as strengthening bars) were usually obtained by joining several pieces [5,6,7]. The edges of the bars to join were heated to a temperature below the melting point and then hammered together to create an integral, homogeneous joint. Before welding, the edges were shaped in order to guarantee the largest contact area between the two pieces, more effective pressing force and hence a better connection [8,9]. Based on these premises, defects at the micro- and meso-scale that are inherent to the reduction process can be identified in historical metal components, as can flaws at the macro scale due to forging. Both of them influence the mechanical behaviour of the element and hence its structural performance.

Tie-rods from Milan Cathedral represent an extremely interesting example of historical metallic components. The building of the cathedral on a former Christian complex started in 1386 from the apses and the choir in the east. It continued through the edification of the transept with the tiburio and dome, which was followed by the erection of the five naves and the spires from east to west. The Cathedral was completed at the beginning of the 19th century with the construction of the façade [10]. Compared to tie-rods in other historical buildings, the structural elements examined have significantly larger cross-sections: the average dimensions are 83x55mm^2. Their length ranges from 5.1 m to 16.4 m depending on the nave. Tie-rods were placed from the beginning of the construction at the springer of every arch and hence most of them have been active for over 500 years. The structural system of the church shows some very interesting peculiarities making even more crucial the structural role of tie-rods [11]. Typically, horizontal thrusts are balanced by many bearing elements [12]. In Milan Cathedral, the main elements devoted to this purpose were the tie-rods and the transversal masonry walls above the vaults. Moreover, over the centuries the loads have continuously changed due to both human and environmental factors, causing a redistribution of the loads through the structure [13,14,15].

In May 2009 the deformation monitoring system working inside the cathedral recorded an anomalous verticality variation in pillar 88 compared with the trend of the previous years [16]. Examination of the area concerned revealed the failure of the tie-rod connecting piers 58 and 88, which was then substituted with a modern steel bar. This event showed the need to perform a broad multidisciplinary study on these elements in order to infer the possible causes of failure. Although microclimate monitoring revealed that during the year relative humidity sometimes exceeds the limits set by the current codes for the conservation of metallic components, favouring the occurrence of corrosion [17], evidence of the failure suggest a collapse due to mechanical reasons. The study therefore had three main focuses: a) estimation of the actual tensile stress of the active elements; b) identification of the most detrimental defects through the use of Non Destructive Techniques (NDTs); c) material characterisation.

The dynamic identification method proposed in [18] was implemented in situ on 112 tie-rods in order to estimate their actual state of stress. This provided interesting results, with stress values in the range of 0–150 N/mm^2 [19]. However, this approach can hardly allow to detect the presence of dominant defects, which govern the actual load capacity of the elements. Forged welds are among the most detrimental ones as they constitute discontinuities which span the whole cross-section. The critical nature of forged welds in structural terms makes their identification and monitoring paramount. As no methods specifically designed for this purpose are currently available, several NDTs commonly adopted for the inspection of modern metals were studied in order to evaluate the potential for extending them to the field of cultural heritage [20]. By adapting eddy current testing to this unconventional application, based on a customised probe, it was possible to identify forged welds, which are the dominant defects of Milan cathedral tie-rods [21].

With regard to mechanical properties, a first campaign was performed using standard tensile tests according to EN ISO 6892-1 on eight samples machined from the broken tie-rod [19]. Results showed a very high standard deviation due to the presence of many defects. Specifically, yield stress, tensile strength and elastic modulus were 142 ± 60 MPa, 199 ± 111 MPa and 206 ± 45 GPa, respectively. For this reason, a mechanical characterisation based on fracture properties of the material was considered more reliable and hence Elasto Plastic crack initiation testing was performed according to ASTM E1820-17 on 13 samples machined from both the base material and the material close to a forged weld [20]. The results shed light on the structurally critical nature of forged welds: fracture toughness at these locations was one order of magnitude lower than the fracture toughness of the base material. Density was measured using the hydrostatic weighing method, yielding a result of 7792 kg/m^3. Since most of the techniques for crack detection are electromagnetic methods, the electrical and magnetic properties of the base material were identified as well. The electrical conductivity (ρ) was found to be $(9.1 \pm 0.9) \times 106$ S/m, while the magnetic hysteresis cycles showed a residual induction and coercive force of about 0.859 T and 889.5 A/m, respectively [21].

The studies discussed here were conducted within the above-mentioned broader multidisciplinary investigation concerning the replaced tie-rod from Milan Cathedral. The aim was to characterise the material properties and to study the reason for failures in order to identify any potential structurally critical features. To this end, failure modes were estimated, and microstructural compounds, types of inclusions, incidence of voids and mechanical properties were studied in detail since they may provide insights of fundamental interest.

2. Material and methods

When ancient buildings are analysed, NDTs are usually preferred. In the case at issue, it was possible to perform several Destructive Tests (DTs) because the broken tie-rod removed in 2009 was made available. The studies focused on the portion of the element close to the failure surface. More precisely, the fracture surfaces (samples A1 and A2) and the section adjacent to sample A1 (sample B) were analysed in depth in order to infer the possible causes of failure and to characterise the material. The location of the samples analysed is shown in Fig. 1. Unfortunately, the actual tensile stress of the element before collapse is unknown as extensive dynamic tests were performed later. However, it is interesting to note that the three southward tie-rods located along the same transverse section of the cathedral showed very high tensile stress values (90–110 MPa).

The different techniques listed below were employed in an integrated manner to achieve reliable results.

- Unaided Visual inspection (VI): although it must be combined with more detailed analyses, unaided VI enables preliminary hypotheses on failure modes and material features to be made.
- Stereo Microscopy (SM): preliminary observations were carried out using a NIKON SM Z2800 stereoscope. This made it possible to detect many kinds of inclusions and porosities, to analyse the area close to the crack and to identify the most interesting regions to inspect.
- Light Optical Microscopy (LOM): it was mainly adopted to analyse microstructures and grain size, identify defects, and provide an initial description of the SIs. A LEICA MDR light optical microscope was used.

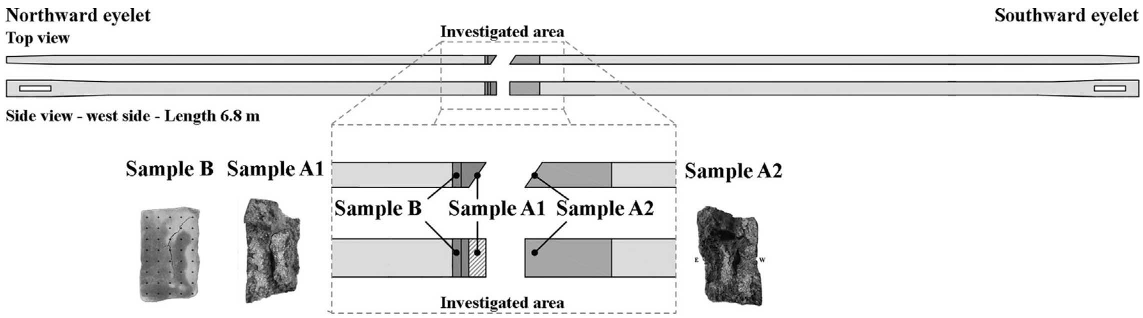

Fig. 1. Location of the investigated samples.

- Scanning Electron Microscopy (SEM): it was performed on many areas of interest identified by other techniques such as SM and LOM in order to detect failure modes at the micro scale, identify microstructural compounds and analyse SIs. Two modes were used, backscattered secondary electrons (BSE) and secondary electrons (SE), to obtain morphological and compositional information respectively.
- Energy Dispersive X-Ray Spectrometry (EDXS): it was combined with SEM to determine the nature of the SIs.
- Vickers hardness test (HV): it was performed with a WOLPERT hardness tester and with a 10 kgf maximum load (HV10) in order to test for a possible correlation between hardness measurements and microstructure and a comparison with literature values.
- Rockwell hardness test (HR): instrumented indentations were performed with a ZWICK HU0.2 tester, with a conical diamond indenter and a preload of 9.8 N, followed by loading up to 200 N. An inverse analysis of results [22] was implemented in order to estimate the local Young's modulus, yield stress, and hardening coefficient values.

3. Results

3.1. Analyses of failure surfaces

Interesting information can be obtained by analysing a tie-rod portion close to the failed section, whose features strongly depend on loading modes, microstructure, temperature and environmental conditions.

Visual inspection and accurate photographical documentation were the first approach to the sample. In Fig. 2 the examined portion of the tie-rod is shown in its location in the cathedral.

The cross-section has different dimensions on the two sides of the failure plane: this suggests that several bars may have been assembled to obtain the entire element. The failure profile is inclined with respect to the tie-rod length.

In Fig. 3, the two fracture surfaces (indicated as sample A1 and sample A2) are shown. They exhibit the typical fibrous appearance of wrought iron, oriented according to the tie-rod length. A visible crack can be observed intersecting both failure surfaces. It takes the form of a large void in the inner part of the cross-section while the tips point outwards. A more deformed zone can be identified on the lower part. A no-planar fracture can be recognised. The surface appears either shiny or oxidised depending on its position on the cross-section. The failure surfaces are extensively oxidised. Dark oxides and red oxides can be distinguished visually.

In order to investigate the indications provided by visual inspection further, the two fracture surfaces were analysed via SEM. Several significant pictures taken over sample A1 are shown in Fig. 4a–c and 5a–c. Similar results were obtained on sample A2. As can be observed in Fig. 4a and Fig. 5a, two areas with different features can be distinguished. Fig. 4b and Fig. 5b reveal the typical transgranular brittle failure through a clear identification of both cleavage planes and river patterns. The cleavage planes indicate the cleaving of the crystals along crystallographic planes. River patterns are formed when the cleavage fracture is forced to re-initiate at the boundary of a grain with a different orientation.

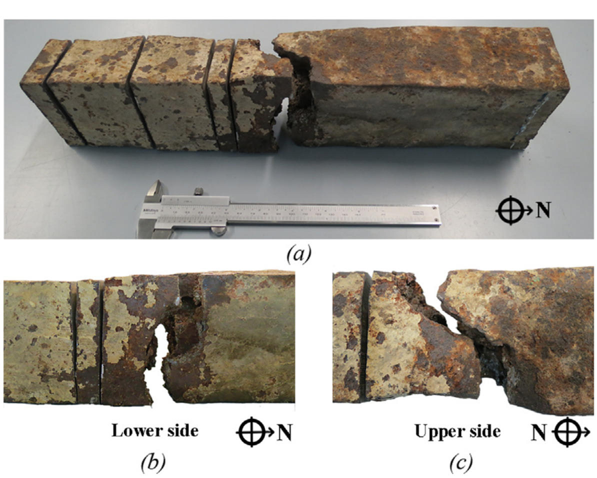

Fig. 2. Investigated portion of tie-rod 59-88, a) general overview, b) enlargement on the broken profiles, lower side, c) enlargement on the broken profiles, upper side.

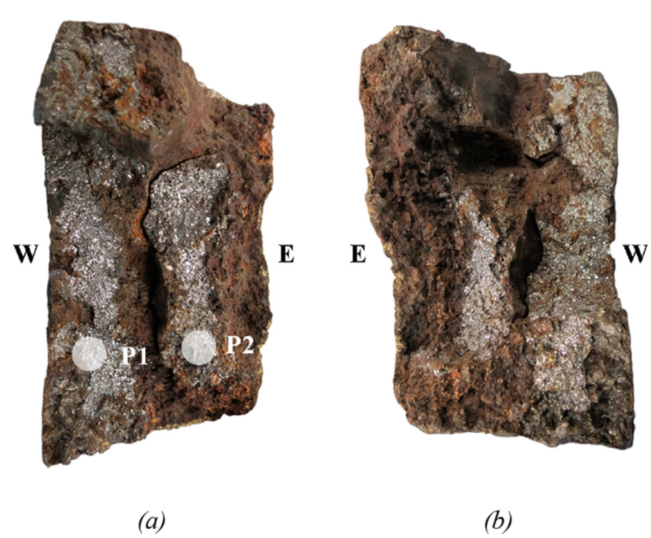

Fig. 3. Failure surfaces and localization of SEM analyses, (a) sample A1 oriented southward, (b) sample A2 located northward.

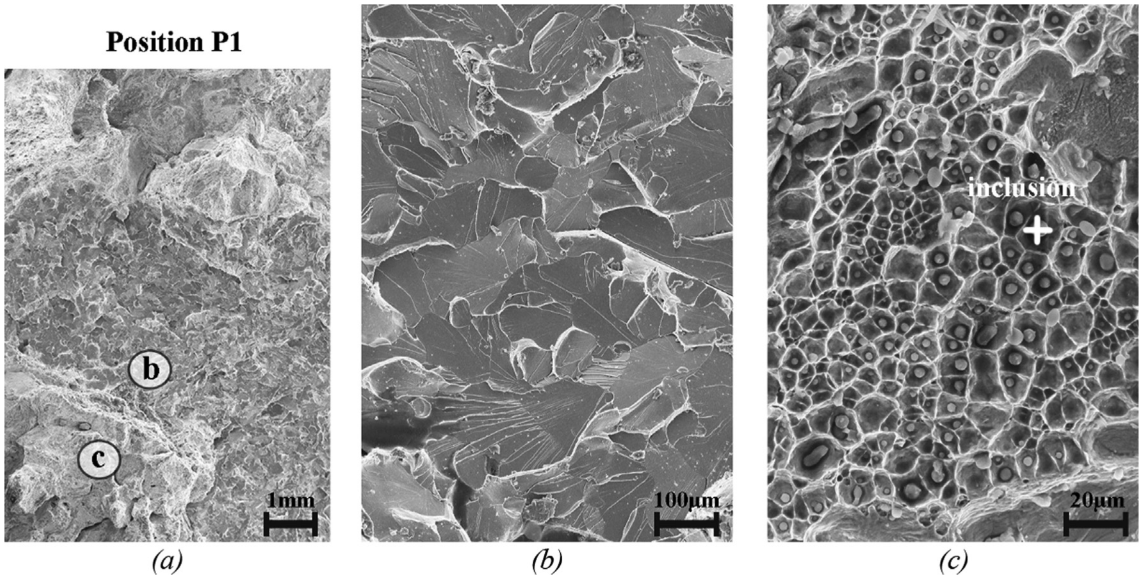

Fig. 4. SEM analyses on sample A1 at position P1. (a) general picture, enlargement on (b) transgranular brittle failure area, (c) ductile failure area.

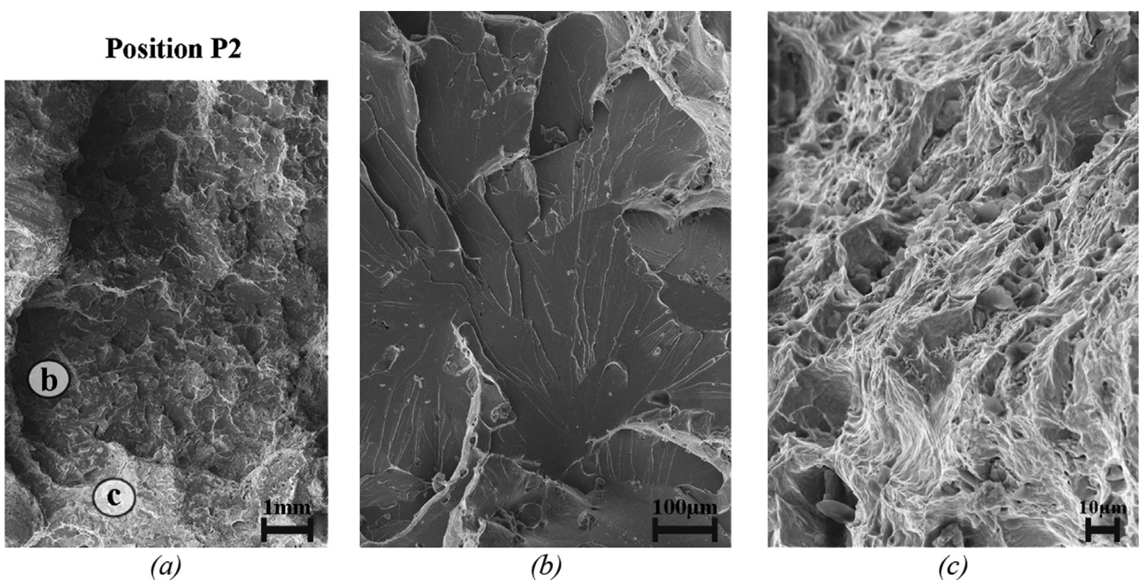

Fig. 5. SEM analyses on sample A1 at position P2. (a) general picture, enlargement on (b) transgranular brittle failure area, (c) ductile failure area.

These tear ridges tend to merge in the direction of crack growth: a downward direction of propagation is suggested. In contrast, Fig. 4c and Fig. 5c clearly show dimples, which indicate a micro-void coalescence around discontinuities such as non-metallic inclusions and impurities. Dimples are symptomatic of a ductile fracture mode. Compositional analysis was performed by EDXS on the inclusion inside a dimple shown in Fig. 4c. As can be seen in Table 1, the main element detected (excluding Fe, C, and O) is Si.

3.2. Microstructural characterisation

Microstructural characterisation was carried out on a cross-section close to the fracture surface (sample B). It was prepared by planar grinding and polishing, according to the ASTM E3-11 Standard Guide for Preparation of Metallographic Specimens [32]. Preliminary inspections of the whole cross-section were performed using the stereo microscope. Several interesting pictures are shown in Fig. 6a–e.

A visible crack crosses the whole specimen. Inside the crack, rust was detected (Fig. 6b and c), suggesting that the crack is not of recent formation. The material is highly defective and many kinds of discontinuities were distinguished, such as porosities, inclusions, macrovoids, and microcracks. Discontinuities of micrometric dimensions or smaller are more concentrated mainly close to the visible crack (Fig. 6a and b). Larger flaws are randomly distributed, especially on the westward portion of the cross-section

Table 1
EDXS compositional semiquantitative analysis on the inclusion inside a dimple.

Elements	O	Na	Mg	Al	Si	P	S	K	Ca	Mn	Fe
Weight [%]	26.4	–	2.0	1.7	13.4	3.4	–	–	4.8	7.3	Bal.

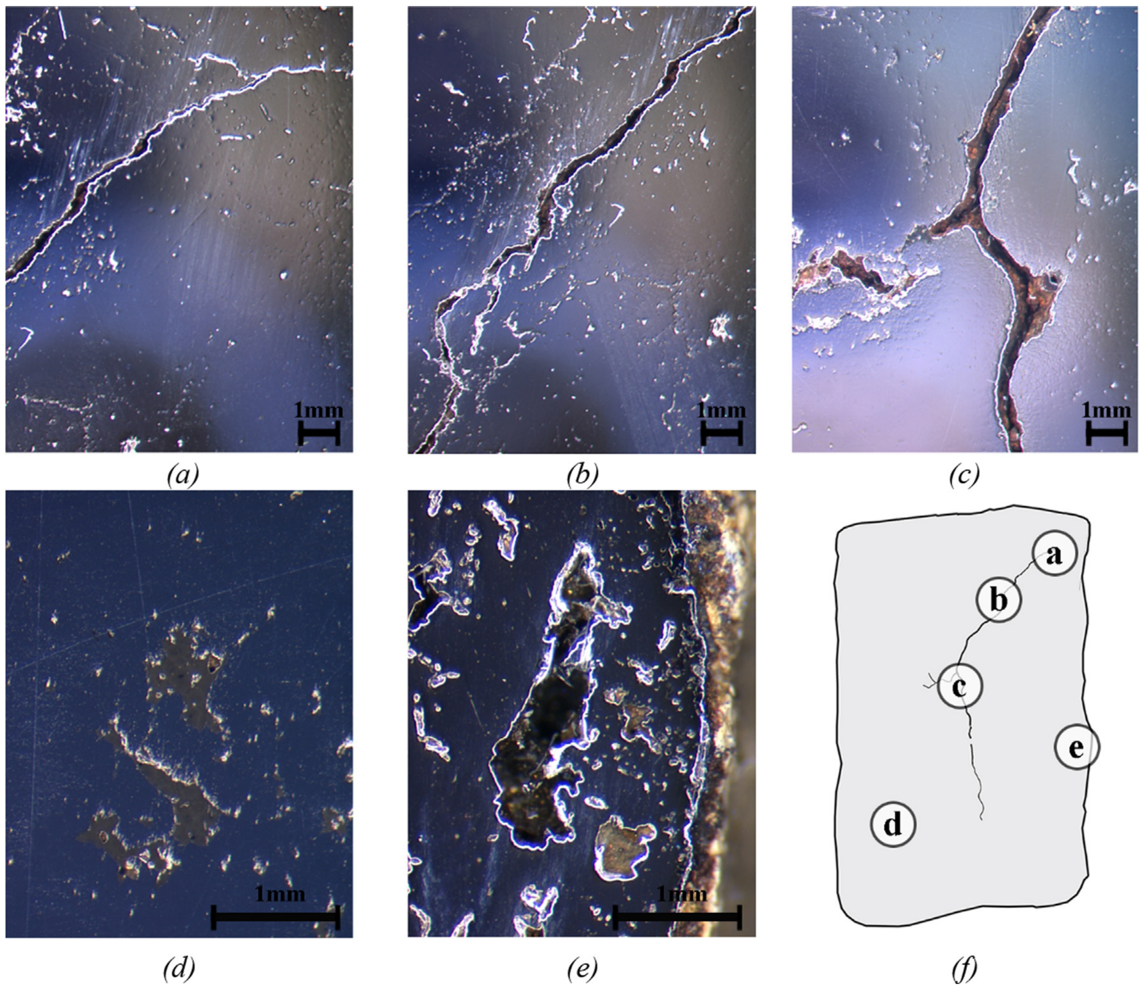

Fig. 6. Stereomicrographs on sample B (a) crack tip, (b) concentrated discontinuities close to the main crack, (c) crack bifurcation, (d) isolated discontinuities, (e) hammerslag layer and voids (f) localization of pictures.

(Fig. 6d). A 0.2–0.3 mm-thick hammerslag layer (oxide produced during hot working) covers the tie-rod (Fig. 6e). It is almost uniform and coherent with the wrought iron core and has probably had a protective effect against corrosion. Very large voids are located below the crust at a depth of up to 15 mm.

After stereo analysis, metallographic etching was carried out on the surface inspected by using nital 2% (solution of nitric acid in ethyl alcohol) in order to reveal the microstructure according to ASTM E407-07 (2015) Standard Practice For Microetching Metals and Alloys [33].

As other studies, including [6], have suggested, some preliminary qualitative insights can be obtained by observing the etched section, the superficial features of which depends on the carbon content. Usually the areas with a carbon content of over 0.2–0.3% appear more opaque. This indication allows an initial distinction to be made at the macro scale between regions characterised by different carburisation states. As Fig. 7b shows, three different conditions can be distinguished:

- 35% of the surface has a C content lower than or equal to 0.2%;
- 20% of the surface has a C content ranging from 0.4% to 0.2%;
- 45% of the surface has a C content greater than or equal to 0.4%.

3.2.1. Metal matrix

LOM analysis confirmed the macroscopic observations. Two main microstructures were identified, namely ferrite and pearlite, and their percentage over the sample is not uniform. In order to coordinate the results provided by different techniques, a grid of 40 points, with a spacing of 10 mm, was traced (Fig. 8).

Micrographs at 100X were taken at each node. Fig. 9a–g show several of the microstructures identified. The fractions of the microstructural compounds were determined according to ASTM E 562-02 Standard Test Method for Determining Volume Fraction by Systematic Manual Point Count [34]. A highly heterogeneous distribution of the two main microstructural compounds was observed: the percentage of pearlite ranges from 97% (Fig. 9c) to 0% (Fig. 9f). The grid nodes were classified into three categories depending on the percentage of pearlite (Table 2). The discrete data system was transformed into a continuous distribution by interpolating the nodal values and the results were plotted in the coloured contour map shown in Fig. 9. An examination of the LOM micrographs reveals that ferrite nucleates at the grain boundary and grows with lamellar shape. Especially in Fig. 9d, Widmanstätten plates can be observed. In addition to ferrite and pearlite, cementite was occasionally detected (Fig. 9b and e).

The area close to the macroscopic crack was also analysed in detail. Fig. 10a and b are illustrative pictures taken by optical microscope before and after etching, respectively. Concentrated inclusions and a sudden change of both microstructure and grain size can be observed across the crack.

3.2.2. Analysis of slag inclusions

With regard to SIs, before the industrial revolution, both wrought iron and steel working were performed at temperatures

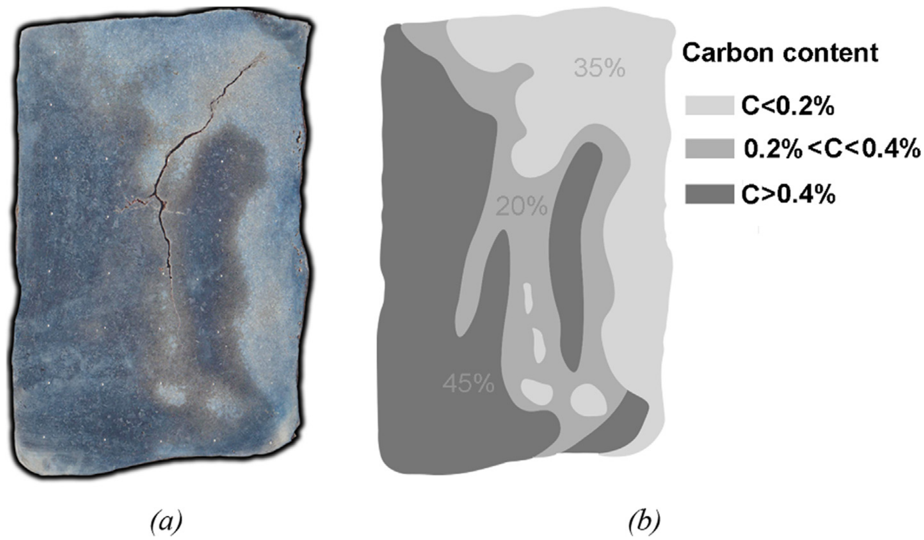

Fig. 7. Carbon content evaluation at the macroscopic level (a) real surface after etching, (b) categorization of the cross-section area.

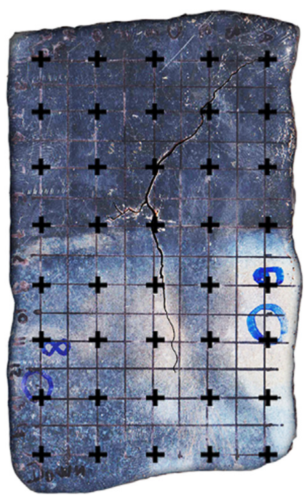

Fig. 8. Reference grid.

below the melting point of iron and hence different types of non-metallic particles remained entrapped in the metallic matrix. They were typically identified by stereoscopic analysis but sometimes could not be easily distinguished from small voids. With the advent of LOM it became possible to identify SIs in the ferrite matrix with certainty and inspect their features. Two examples are shown in Fig. 11a and b. Both of them are iron-rich inclusions. Fig. 11a illustrates a bulky two-phase SI of wüstite and glass, while Fig. 11b depicts a slender two-phase SI of fayalite and glass.

In contrast, SIs in the pearlite matrix cannot be easily distinguished from voids using LOM. Therefore, in order to characterise them properly, SEM analysis coupled with EDXS was used. After obtaining a complete overview of the whole cross-section, four significant points were chosen to perform SEM analyses:

- close to the upper tip of the visible crack (pearlite 60% and ferrite 40%, Fig. 12a);
- close to the widest part of the visible crack (pearlite 62% and ferrite 38%, Fig. 12b);
- undamaged material (pearlite 0% and ferrite 100%, Fig. 12c).
- close to the lower tip of the visible crack (pearlite 20% and ferrite 80%, Fig. 12d).

At the same position, BSE often revealed the presence of different types of SIs. Each one of them was studied by EDXS. The results are reported in Table 3.

The pictures in Fig. 12a and b were taken of material characterised by approximately the same percentage of ferrite and pearlite. Different types of inclusions were revealed. In Fig. 12a, the particularly high percentage of Si (about 63%) at the A-inclusion suggests a glassy SI (iron content is negligible). In contrast, the chemical analysis of the B-inclusion in Fig. 12a and the C-inclusion in Fig. 12b suggests an iron-rich glassy composition. As expected, inclusions of rust were identified inside the crack (D-inclusion in Fig. 12a), as indicated by the detection of mostly Fe and O.

In Fig. 12c, the metal matrix is pure ferrite (0% pearlite). The detected inclusion has a bulky shape and a pale dendritic phase with a glassy appearance. EDXS analysis reveals a Fe-rich inclusion with a significant amount of Si (13.10%). More specifically, it is characterised by dendrites of wüstite (FeO) in a glassy matrix. There is also a significant presence of Ca and Mn, the content of which is 4.75% and 6.33%, respectively. Carbon is completely absent. The morphology is very similar to inclusions in Fig. 11, as detected by LOM. Indeed, the same metal matrix surrounds it.

The picture in Fig. 12d shows the mostly ferritic microstructure (80% ferrite and 20% pearlite). EDXS on the F-inclusion revealed iron oxides, as in the other inclusion analysed inside the crack. The G-inclusion is spheroidal graphitic carbon, the enlargement of which is shown in Fig. 12e. Its size is about 10–15 µm. This kind of inclusion is recurring in the mostly ferritic iron part of the sample. Around nodules, a finer pearlite can be usually found, becoming progressively coarser. H-inclusion in Fig. 13d is iron-free, with high percentage of Si, Ca, and Mn.

3.2.3. Hardness tests

Vickers and Rockwell hardness tests were carried out on the polished surface by conforming to the same grid used for the optical microscope observation. The two measurements were reciprocally shifted by 4 mm in order to avoid any interaction. As expected, in the mostly pearlitic structure the indenter produces local cracking around the indentation area, while in the mostly ferritic structure only local plastic deformation occurs. This confirms

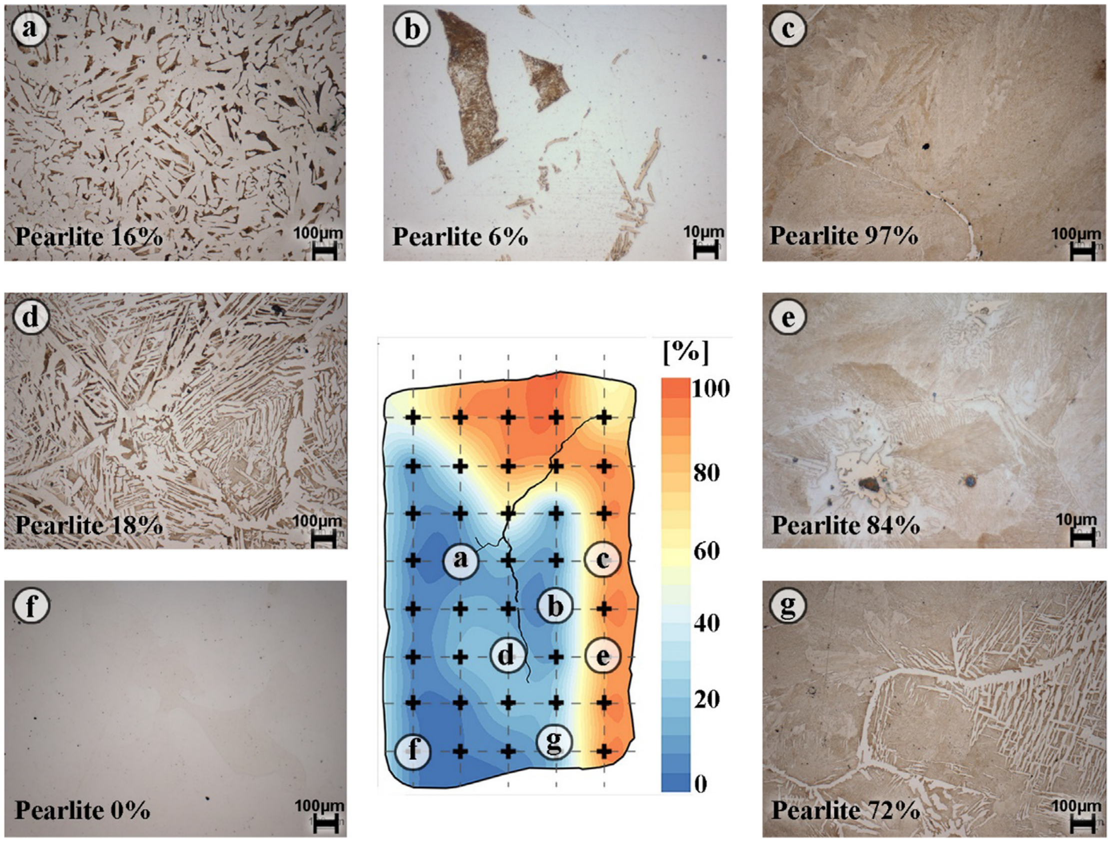

Fig. 9. Detected metal matrix via LOM (a) pearlite 16%, (b) pearlite 6%, (c) pearlite 97%, (d) pearlite 18%, (e) pearlite 84%, (f) pearlite 0%, (g) pearlite 72%,(h) pearlite distribution and micrographs locations.

Table 2
Grid node classification according to the pearlite percentage.

Microstructure type	Pearlite content	Investigated points
Mostly pearlitic structure	>75%	12.5%
Ferritic – pearlitic Structure	75–25%	10.0%
Mostly ferritic structure	<25%	77.5%

the different material properties over the cross-section, which may be more brittle or more ductile depending on microstructure. The discrete Vickers and Rockwell hardness data were converted into coloured contour maps, which are reported in Fig. 13a and b respectively.

The Vickers hardness values fall within the 79-284HV10 range and have a mean value of 132HV10 (standard deviation 55HV10). The Rockwell hardness values range from a maximum of 79HR to a minimum of 50HR and have a mean value of 61HR (standard deviation 9.2HR). The large difference between the minimum and maximum values suggests that the penetrator alternately delved into softer and harder phases. Therefore, characteristic Vickers hardness values of pearlitic, ferritic, and ferritic-pearlitic structures were estimated by classifying the grid nodes as follows:

- 100% pearlite;
- almost 50% ferrite and 50% pearlite;
- 100% ferrite.

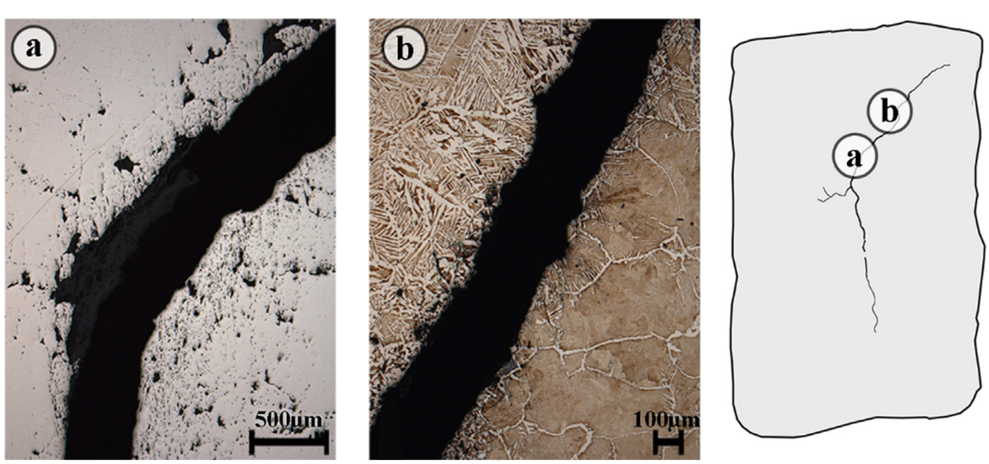

Fig. 10. Microstructure close to the visible crack (a) concentrated discontinuities, (b) sudden microstructure changes (c) micrographs localization.

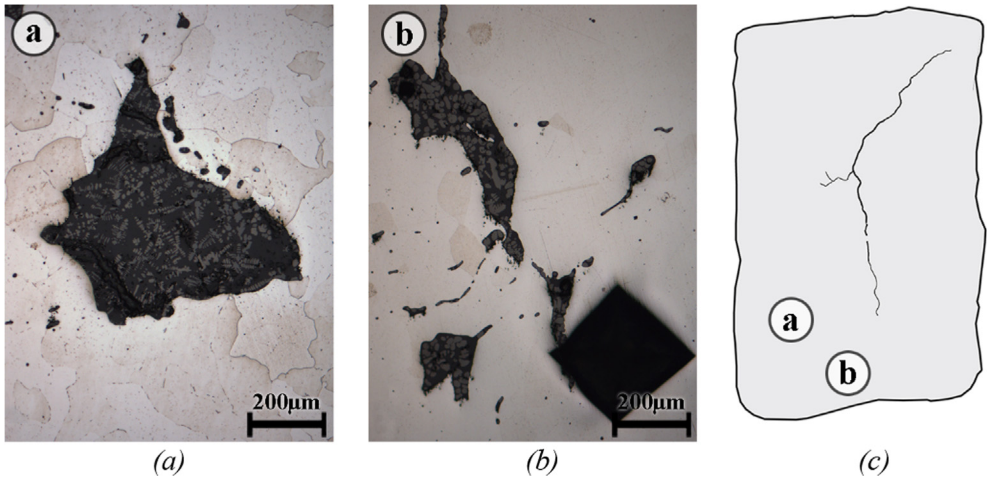

Fig. 11. LOM analyses on the two-phase inclusions detected in ferrite matrix. (a) wüstite and glass, (b) fayalite and glass, (c) micrographs localization.

Since the variability in these subintervals is low, the average values can be assumed as the representative values for the metal matrix considered. According to this procedure, ferrite could be associated with 94HV10, pearlite-ferrite with 148HV10, and pearlite with 223HV10.

A 3D micro geometrical survey was performed using the ALICONA Infinite Focus 3D optical microscope inside the indentation imprint of points exceeding the intervals defined by mean value and standard deviation and iron-free glassy inclusions were detected.

An inverse analysis was performed at each location where hardness was measured, exploiting the pertinent indentation curve as input data in order to estimate the material parameters governing the mechanical behaviour such as Young's modulus, yield strength and hardening coefficient. As discussed in [23] the estimation of these values is not convincing because the estimated Young's modulus fell within a reasonable range of 180–220 GPa only in four nodes. This could be explained by the strict assumptions underlying the method, namely isotropic and homogeneous material with a grains size at least two orders of magnitude smaller than the dimension of the indentation imprint and characterised by linear elasticity and exponential hardening law in the plastic stage [24 25]. As a matter of fact, these conditions are not appropriate for the examined material.

4. Discussion

The two failure surfaces provide interesting information about the failure mechanism. Dark oxides are usually produced at the forging temperature and hence are a result of the manufacturing process; red oxides, commonly known as "rust", form at room temperature. The latter are fairly evenly distributed over the whole cross-section and are caused by atmospheric corrosion. This evidence is in agreement with the results of microclimate monitoring [17], which revealed that for most of the year relative humidity exceeds the recommended limit of 50%, favouring the onset of corrosion in metallic materials. However, the characteristics of the fracture surfaces, as well as the generalised corrosion itself, indicate a failure that was mainly determined by mechanical properties, defectiveness and load conditions. It is reasonable to assume that the crack nucleated inside the section in a weaker region of the material of sizable dimensions (~5–8 mm), where local stress concentration occurred. The position of the visible crack across the specimen slices suggests an inclined propagation relative to the tie-rod length. Non-homogeneous mechanical properties can be inferred from the appearance of the failure surfaces. This hypothesis is confirmed by SEM analyses revealing both brittle and ductile collapse mechanisms. The former is associated with the shiny cross-section surface while the latter is associated with the more opaque part. The remarkable heterogeneity of the material and the presence of silica oxides suggest iron smelting in a low-reducing, non-homogeneous atmosphere. As noted above, these conditions may be associated with older furnaces, based on the direct method of reduction.

The differences in the amount of carbon in the cross-sections can be accounted for by poor hot working resulting from handwork. However, the level of carburisation is relatively high compared with values measured in the tie-rods of other churches of the same period [26]. This aspect can be attributed to the employment of highly qualified blacksmiths due to the importance of Milan Cathedral. The evaluation of carbon content evaluation at the macroscopic level as displayed in Fig. 8b can be completely overlapped with the observations made at the microscopic scale. The most highly carburised part of the cross-section corresponds to the mostly pearlitic microstructure, which has a higher carbon content than the ferritic matrix. More generally, the distribution of the main microstructural compounds, i.e. ferrite and pearlite, indicates a highly heterogeneous material, confirming the hypothesis regarding the furnace based on the analysis of the fracture surface. These items of evidence are confirmed in the literature by many authors, including [27] [3] and [6]. However, the mostly ferritic metal matrix is prevalent and corresponds, as expected, to the most highly deformed portion of the cross-section (higher ductility). Grain boundaries can be clearly identified only where the same amount of ferrite and pearlite occurs. They have large sizes (hundreds of microns), but their dimensions are extremely heterogeneous. Widmanstätten plates can be observed in these regions as well. The formation of this particular microstructure is highly dependent on the chemical composition of the bloom and the cooling temperature. Specifically, it can be recognised in low carbon content material and indicates a very high forging temperature (950 °C–1100 °C), followed by a rapid cooling process. It is typical of wrought iron produced by the direct process [28].

The heterogeneity of the material is also related to its inherent defectiveness. A stereoscopic examination provides a general overview of the distribution of defects. However, at this inspection scale it was not possible to distinguish their features. LOM and SEM enabled larger inclusions (200 μm) detected in the mostly ferritic microstructure to be characterised. As shown in Fig. 12, there are two different types of iron-rich two-phase inclusions. Both of them suggest the use of the direct method of reduction;

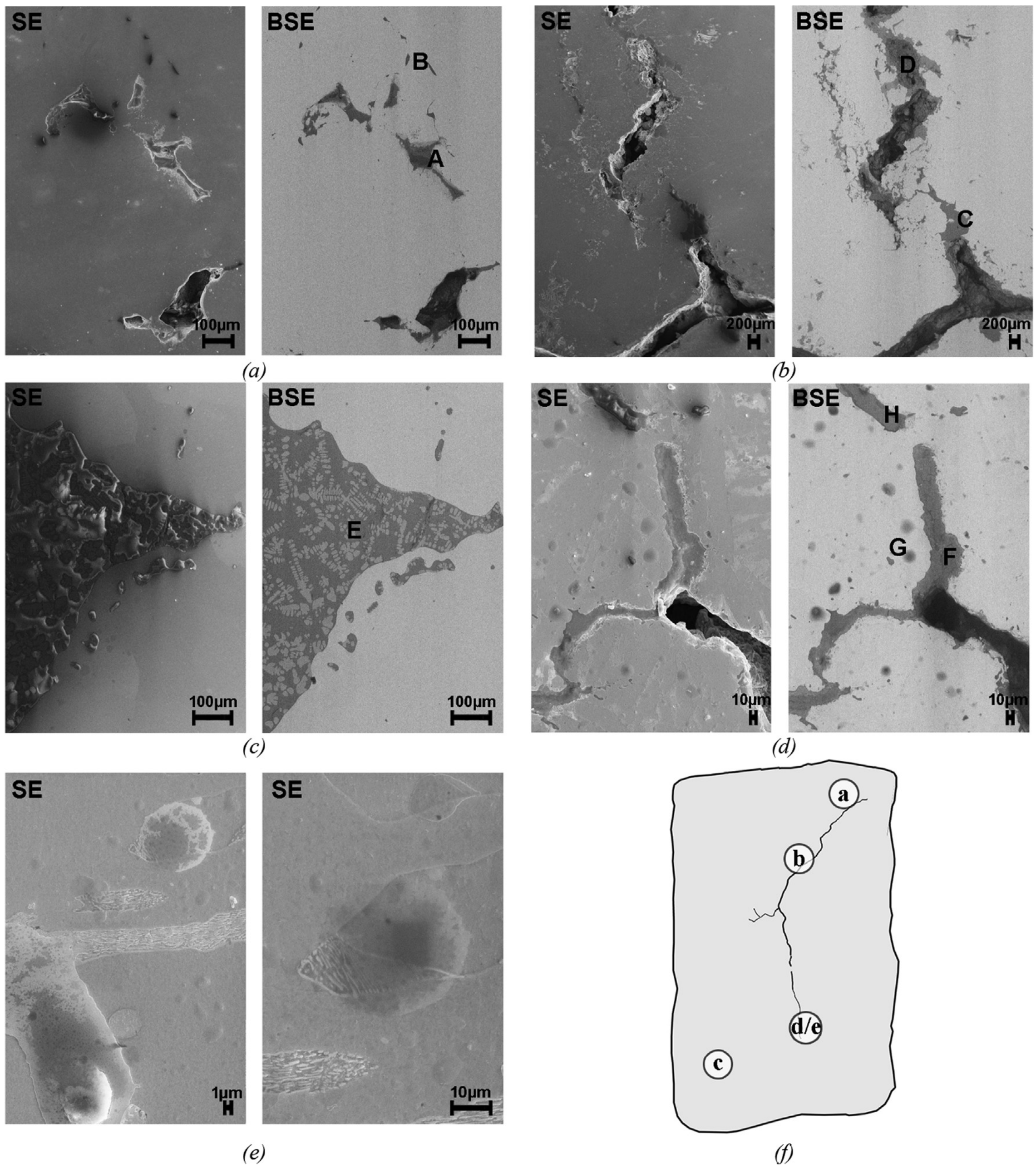

Fig. 12. SEM analysis, SE mode and BSE mode with EDXS localization on different metal matrix. (a) pearlite 60% and ferrite 40%, (b) pearlite 62% and ferrite 38%, (c) pearlite 0% and ferrite 100%, (d) pearlite 20% and ferrite 80%, (e) enlargements on carbon nodules, (f) micrographs location.

Table 3
Semi-quantitative compositional analyses on inclusions (SEM, EDXS, Wt%). The analysis of carbon shall be considered qualitative.

		C	O	Na	Mg	Al	Si	P	S	K	Ca	Mn	Fe
Fig. 12a Pearlite 60% Ferrite 40%	A	35.8	–	–	–	–	62.7	–	–	–	–	–	Bal.
	B	–	13.8	1.0	0.8	3.2	18.2	1.0	0.3	1.8	2.1	–	Bal.
Fig. 12b Pearlite 62% Ferrite 38%	C	–	38.0		3.4	3.7	28.3	–	0.8	3.5	10.1	9.7	Bal.
	D	–	29.3	1.5	–	–	–	–	–	0.8	–	–	Bal.
Fig. 12c Pearlite 0% Ferrite 100%	E	–	22.9	–	1.7	1.8	13.1	0.7	0.e 1	1.4	4.8	6.3	Bal.
Fig. 12d Pearlite 20% Ferrite 80%	F	39.0	29.3	–	–	–	1.3	–	1.8	0.6	–	–	Bal.
	G	51.0	9.3	1.2	–	–	0.2	–	–	0.4	–	–	Bal.
	H	29.1	28.0	–	1.8	2.8	18.5	–	0.2	2.2	7.2	7.5	Bal.

any differences probably arose from the local thermodynamic conditions inside the furnace. The fayalite glass inclusions usually result from higher reducing atmosphere than the other type of dendritic slag. Inclusions embedded in the mostly pearlitic metallic matrix were investigated only by SEM because they have smaller dimensions (50 μm) and hence cannot be identified by LOM. They generally show a greater amount of Si, causing greater brittleness. This evidence confirms the shiny appearance of the fracture

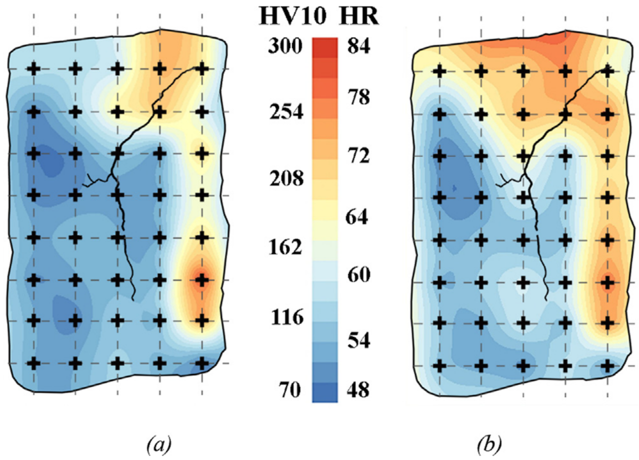

Fig. 13. Hardness values distribution, a) Vickers HV10, b) Rockwell HR.

surfaces. The main difference between the A-inclusion in Fig. 13a and the D-inclusion in Fig. 13b is the relatively high content of Ca (10.14%) and Mn (9.66%) in the latter, which usually originates from ashes and ore, respectively. Carbon-rich inclusions and rust were identified as well. As the percentage of ferrite increases, the amount of Si decreases and iron-rich inclusions are more frequent. This correlation between metal matrix and type of slag is confirmed in the literature, as shown in [29] and [30].

The microstructural findings in terms of matrix and types of inclusions show a strong agreement with the hardness testing results. The distribution of Vickers and Rockwell hardness values can be completely overlapped with the pearlite content map: higher hardness values correspond to the mostly pearlitic microstructure with mainly silica-rich inclusion while the lowest ones correspond to the mostly ferritic microstructure with iron-rich inclusions. With regard to hardness values, the comparison with similar case studies is not meaningful because small differences in the metal matrix as well as in grain dimensions may strongly influence the results.

All of the evidence from analyses at different inspection scales leads to the hypothesis of the direct reduction method. Nevertheless, slag inclusions recognised in other similar cases [27] are usually much larger than those identified in the Milan Cathedral tie-rod. It is reasonable to assume the use of a more accurate metalworking process due to the relevance of the building. Indeed, the fracture characterisation that was performed [31] reveals an extremely tough base material. A hardening branch without local instabilities dominates the load-displacement curve, plastic deformations are extremely marked and the ultimate strength is never reached in the strain range allowed by the test. The same study demonstrates that the mechanical performance of the material decreases sharply at forged welds due to the heat treatment used. In samples including forged welds, the load-displacement curve shows a softening branch and an unstable crack propagation associated with the presence of local discontinuities. The resulting toughness values are about one order of magnitude lower than the base material. For this reason, forged welds can be considered the most critical cross-sections. This evidence cannot be directly extended to all historical tie-rods, as it depends on the average dimensions of slag inclusions.

The tie-rod failure analyses of the replaced element confirm this insight. The crack propagated along an inclined direction with respect to the longitudinal tie-rod axis, recalling the typical forged weld shape. Moreover, the crack visible over the cross-section is located across a region where concentrated discontinuities and sudden change of microstructure occurred, as shown via LOM before and after etching. As mentioned previously, in the literature these two occurrences are often associated with the presence of forged welding of two wrought-iron pieces [6]. This evidence, combined with the results of visual inspection, leads to the hypothesis of crack propagation along a forged weld, which is in agreement with the lower toughness observed at these locations.

5. Conclusions

The behaviour of wrought iron tie-rods in historical buildings is strongly affected by heterogeneity and defectiveness in the material stemming from the manufacturing techniques used. In this paper, the case study of the Milan cathedral tie-rods was addressed. Many analyses were conducted at different inspection scales in order to infer possible causes of tie-rod failure in connection with metallurgical features of the material.

Many observations led to the hypothesis that tie-rod failed due to a crack initiating inside the cross-section at a weaker point (macroscopic inclusion or void) and propagating outward along a forged weld. Crack morphology on the examined cross-section and along the tie-rod length indicates the direction of propagation. Concentrated inclusions and sudden variations of microstructure across the crack highlighted via LOM suggest the presence of a forged weld. Lower toughness values at this region achieved by the mechanical characterisation described in [31] confirm this mentioned insight. Moreover, the macroscopic crack detected in another tie-rod substituted in 2014 exhibits the same straight-scarf forged weld shape. This evidence endorses the results of the present study.

Failure mode is not homogeneous and both transgranular brittle and ductile failures were identified over the fracture surfaces. Brittle and ductile failure modes were identified very close to one another. Ductile failure corresponds to the most highly deformed part identified through the visual inspection.

These insights are in agreement with the microstructural findings. The material is extremely heterogeneous in terms of both microstructural compounds and defects. Although ferrite and pearlite are the prevalent microstructures, their distribution over the cross-section is extremely variable. Two distinct more homogenous areas can be identified, corroborating the hypothesis of different mechanical properties over the investigated cross-section. Across their boundary, microstructure and grain size suddenly change, two pieces of evidence which substantiate the hypothesis of a forged weld between two bars at this location. More generally, the mostly ferritic structure is prevalent and characterises 78% of the examined grid nodes. As the percentage of pearlite content increases, the amount of carbon increases, and hence also strength and brittleness. With regard to defects, different types of flaws resulting from the manufacturing process were identified, such as microcracks, micro-porosities, voids and slag inclusions. A strong correlation was found between the identified microstructures (ferrite, pearlite) and the type of discontinuities. Iron-rich dendritic slag inclusions (typically wüstite) characterise the ferritic matrix. Spheroidal graphitic carbon was identified in regions where the ferritic structure is prevalent. Fine pearlite nucleates around carbon nodules. These two types of inclusions are completely absent from the mostly pearlitic structure, where smaller glassy slags were detected. Microcracks were identified as well. Usually inside cracks iron oxide inclusions were recognised.

Both microstructural compounds and defects strongly affect mechanical properties. Indeed, metallurgical characterisation shows a strong agreement with the results of hardness tests. Data variability confirms the heterogeneity of the material. Higher hardness values were found in the primarily pearlitic microstructure, while the lowest values were observed mostly in the ferritic microstructure. Distinctive hardness values related to pearlitic, ferritic and ferritic-pearlitic structures were estimated. They correspond to 76HR, 65HR and 54HR respectively. Abnormally high hardness values usually correspond to the presence of silica inclusions inside the indentation imprint, which are harder than the surrounding material.

Metallurgical characterisation was carried out on one tie-rod because other broken elements were not available. Despite the inevitable heterogeneity of the material arising from the use of the direct reduction method and manual forging, the most significant findings of this study can be reasonably extended to all the other elements of the cathedral because they are characterised by analogous geometry and were obtained from the same metalworking process. Nevertheless, the availability of data collected from other elements of Milan Cathedral would probably make it possible to perform statistical analyses to confirm this insight systematically. Although many types of defects were recognised, not all of them have the same consequence for the behaviour of the element. Defects at the microscale are relatively uniformly distributed and involve an average decrease in mechanical properties, such as stiffness. In contrast, forged welds may entail a significant reduction in the resistant cross-section and high strain localisation and hence are more dangerous. Therefore, in tie-rods that are comparable to the one examined in this case study it is reasonable to assume that failure is more probable at these critical sections.

This observation cannot be directly extended to tie-rods in other churches from the same period, however. Smaller cross-sections make it easier to obtain a more uniform joint during hot-forging. Moreover, a higher incidence of larger inclusions is to be expected in less important construction sites, where less skilled labour was employed generally used. In such conditions, forged welds may not be the most detrimental defects and failure may occur due to crack propagation at an internal macroscopic SI.

Nevertheless, the analyses conducted in the course of this research make an interesting contribution to wider knowledge of ancient tie-rod material. They highlight the importance of recognising critical defects within the inherently high defectiveness of ancient wrought iron. This also calls for the design of customised non-destructive diagnostic methods able to detect them.

Declaration of Competing Interest

None.

References

[1] R.F. Tylecote, A History of the Metallurgy, Institute of Materials, London, 1992.
[2] C. Mapelli and W. Nicodemi, The Civilisation of Iron: from prehistory to the third millenium, Milano: Olivares, 2004.
[3] A. Disser, P. Dillmann, C. Bourgain, M. L'Héritier, E. Vega, S. Bauvais, e M. Leroy, Iron reinforcements in Beauvais and Metz Cathedrals: from bloomery or finery? The use of logistic regression for differentiating smelting processes, J. Archaeol. Sci. 42 (2014) 315–333.
[4] M. Cohen, D. Ashkenazi, A. Stern, Y. Kahanov, e D. Cvikel, Iron artefacts from the Akko Tower Wreck, Israel, and their contribution to the ship's characterization, Archaeol. Anthropological Sci. 9 (6) (2017) 1243–1257.
[5] P. Fajfar, J. Medved, G. Klančnik, T. Lazar, M. Nečemer, e P. Mrvar, Characterization of a Messer–The late-Medieval single-edged sword of Central Europe, Mater. Charact. 86 (2013) 232–241.
[6] G. Pagès, P. Dillmann, P. Fluzin, e L. Long, A study of the Roman iron bars of Saintes-Maries-de-la-Mer (Bouches-du-Rhône, France). A proposal for a comprehensive metallographic approach, J. Archaeol. Sci. 38 (6) (2011) 1234–1252.
[7] A. Aronson, D. Ashkenazi, O. Barkai, e Y. Kahanov, Archaeometallurgical investigation of the iron anchor from the Tantura F shipwreck, Mater. Charact. 78 (2013) 108–120.
[8] G. Musso and G. Copperi, Particolari di costruzioni murali e finimenti di fabbricati: Parte 1: Opere muratorie [Detail of masonry construction and finishing of building: Part 1: Masonry works], 3 riveduta ed accresciuta ed., Torino: G.B. Paravia e comp. 1887.
[9] I. Andreani, L'arte nei mestieri. 2: Il fabbro [The art in craft: the blacksmith], Milano: Hoepli, 1998.
[10] Fabbrica del Duomo di Milano, Annali della Fabbrica del Duomo di Milano dall'origine fino al presente [The annals of Fabbrica del Duomo from the origins till the present], Milano: G. Brigola, 1877
[11] C. Ferrari da Passano, Il Duomo rinato [Milan cathedral reborn], Vigevano: Diakronia, 1988.
[12] J. Heyman, The Stone Skeleton: Structural Engineering of Masonry Architecture, Cambridge University Press, Cambridge, 1997.
[13] D. Coronelli, C. di Prisco, F. Pisanò, S. Imposimato, S. Ghezzi e M. Pesconi, «The tiburio of the Cathedral of Milan: structural analysis of the construction and the 20th century foundation settlements,» in Structural Faults and Repair 2014, Milano, 2014.
[14] D. Coronelli, B. Caggioni, e F. Zanella, The Cathedral of Milan: the structural history of the loadbearing system, Int. J. Archit. Heritage 9 (4) (2015) 510–528.
[15] G. Cardani, D. Coronelli, G. Angjeliu, Damage Observation and Settlement Mechanisms in the naves of the Cathedral of Milan, Structural Analysis of Historical Constructions: Anamnesis, Diagnosis, Therapy, Controls, Proceedings of the 10th international conference on structural analysis of historical constructions, Belgium Leuven, 2016.
[16] A. Giussani, Relazione sulle misure eseguite per il controllo delle deformazioni del Duomo di Milano nei giorni 21, 23 e 28 Novembre 2011 [Report on deformation monitoring in the Cathedral of Milan on dates 21, 23 and 28 November 2011], Politecnico di Milano, Lecco, 2011.
[17] N. Aste, R.S. Adhikari, M. Buzzetti, S. Della Torre, C. Del Pero, e F. Lonforte, Microclimatic monitoring of the Duomo (Milan Cathedral): risks-based analysis for the conservation of its cultural heritage, Build. Environ. 148 (2019) 240–257.
[18] N. Tullini, F. Laudiero, Dynamic identification of beam axial loads using one flexural mode shape, J. Sound Vib. 318 (1) (2008) 131–147.
[19] M. Vasic, A multidisciplinary approach for the structural assessment of historical constructions with tie-rods PhD thesis, Milano: Politecnico di Milano, 2015.
[20] M. Bellanova, e R. Felicetti, A multidisciplinary strategy for the inspection of historical metallic tie-rods: the milan cathedral case study, Int. J. Archit. Heritage 13 (3) (2019) 371–389.
[21] M. Bellanova, M. Carboni, e R. Felicetti, Eddy current testing to the detection of the most detrimental defects in historical metallic tie-rods, NDT & E Int. 104 (2019) 34–41.
[22] G.F. Bocchini, B. Rivolta, G. Silva, E. Poggio, M.R. Pinasco, e M.G. Ienco, Microstructural and mechanical characterisation of some sinter hardening alloys and comparisons with heat treated PM steels, Powder Metall. 47 (4) (2004) 343–351.
[23] M. Bellanova, A. Baggioli, B. Rivolta, R. Felicetti, e A. Cornaggia, Metallurgical and Mechanical Characterization of the Historical Tie-Rod of Duomo di Milano, XXXI° International Conference of Cultural heritage, Brixen, 2015.
[24] V. Buljak, e G. Maier, Proper orthogonal decomposition and radial basis functions in material characterization based on instrumented indentation, Eng. Struct. 33 (2011) 492–501.
[25] G. Maier, V. Buljak, T. Garbowski, G. Cocchetti, e N. Giorgio, Mechanical characterization of materials and diagnosis of structures by inverse analysis: some innovative procedures and applications, Int. J. Comp. Methods 11 (3) (2014).
[26] M. L'héritier, I. Guillot, P. Dillmann, Microstructural characterization and mechanical properties of iron reinforcements in buildings from the medieval and modern periods in France, Int. J. Archit. Heritage 13 (3) (2019) 507–519.
[27] C. Calderini, P. Piccardo, e R. Vecchiattini, Experimental characterization of ancient metal tie-rods in historic masonry buildings, Int. J. Archit. Heritage 13 (3) (2019) 425–437.
[28] D. Ashkenazi, E. Mentovich, D. Cvikel, O. Barkai, A. Aronson e Y. Kahanov, «Archaeometallurgical Investigation of Iron Artifacts from Shipwrecks – A Review,» Archaeology, New Approaches in Theory and Techniques, 169-186, 2012.
[29] D. Cvikel, D. Ashkenazi, A. Stern, e Y. Kahanov, Characterization of a 12-pdr wrought-iron cannonball from the Akko 1 shipwreck, Mater. Charact. 83 (2013) 198–211.
[30] P. Dillman, e M. L'Héritier, Slag inclusion analysis for studying ferrous alloys employed in French medieval buildings: supply of materials and diffusion of smelting processes, J. Archaeol. Sci. 34 (11) (2007) 1810–1823.
[31] A. Gianneo, M. Carboni, M. Bellanova, e R. Felicetti, Study on the influence of defects on the strenght of metallic historical tie-rods, in 12th International Conference on non-destructive investigations and microanalysis for the diagnostics and conservation of cultural and environmental heritage (Art.17), Turin, November 22nd/24th, 2017.
[32] ASTM E3-11 , Standard Guide for Preparation of Metallographic Specimens.
[33] ASTM E407-07 (2015), Standard Practice For Microetching Metals and Alloys.
[34] ASTM E 562-02, Standard Test Method for Determining Volume Fraction by Systematic Manual Point Count.